Slope deformation, reservoir variation and meteorological data at the Khoko landslide, Enguri hydroelectric basin (Georgia), during 2016-2019

Alessandro Tibaldi[1*], Federico Pasquaré Mariotto[2], Paolo Oppizzi[3], Fabio Luca Bonali[1], Nino Tsereteli[4], Levan Mebonia[5], Johni Chania[5]

[1] Department of Earth and Environmental Sciences, University of Milan Bicocca, 20129 Milan, Italy
[2] Department of Human and Innovation Sciences, Insubria University, Como, Italy
[3] Geolog.ch, Mendrisio, Switzerland
[4] Institute of Geophysics, University of Tbilisi, Tbilisi, Georgia
[5] Enguresi LtD Society, Georgia

***Corresponding Author**: alessandro.tibaldi@unimib.it

Abstract

The Greater Caucasus mountain belt is characterized by deep valleys, steep slopes and frequent seismic activity, the combination of which results in major landslide hazard. Along the eastern side of the Enguri water reservoir lies the active Khoko landslide, whose head scarp zone affects the important Jvari-Khaishi-Mestia road, one of the few connections with the interior of the Greater Caucasus. Here, we present a database of measurement time series taken over a period of 4 years (2016-2019) that enable to compare slope deformation with meteorological factors and man-induced perturbations owing to variations in the water level of the reservoir. The monitoring system we used is composed of two digital extensometers, placed within two artificial trenches excavated across the landslide head scarp. The stations are equipped also with internal and near ground surface thermometers. The data set is integrated by daily measurements of rainfall and lake level. The monitoring system – the first installed in Georgia - was set up in the framework of a NATO-funded project, aimed at assessing different types of geohazards affecting the Enguri artificial reservoir and the related hydroelectrical plant. Our results indicate that the Khoko landslide displacements appear to be mainly controlled by variations in hydraulic load, in turn induced by lake level oscillations. Rainfall variations might also have contributed, though this is not always evident for all the studied period. The full databases are freely available online at DOI: 10.20366/unimib/unidata/SI384-2.0. (Tibaldi et al., 2020).

Eliminato: DOI:

Eliminato: 10.20366/unimib/unidata/SI384-1.1

1 Introduction

Landslides are widespread natural hazard sources, affecting most of the world's countries and capable of causing serious economic losses. In fact, they can damage buildings, communication systems and

the overall environment. Moreover, these natural events are major cause of loss of life (Froude and Petley, 2018). The monitoring of landslides is a necessary step to implement protective measures, as it allows to recognize possible acceleration in slope deformation rate, alert residents or close road communication systems, where needed. This type of monitoring is also of paramount importance for assessing possible triggering factors (Casagli et al., 2009), determining the level of risk (Spiker and Gori, 2003), and planning land use and risk management (Fell et al., 2005; Bertolini et al., 2005). This activity can be of special relevance in case of complex situations, such as those affecting an artificial water reservoir, where water variations can destabilize (or stabilize) the slopes overlooking the basin. In such case, multiparameter data can be crosscut in order to look into possible correlations between lake level variations, meteorological conditions, and slope deformations, which in turn are key to effectively managing the filling and emptying of the reservoir.

The database of slope deformation can be derived from a variety of possible monitoring tools, which range from on-site instruments to remotely controlled ones. The formers include continuous or intermittent data collection, such as settlement gauges, inclinometers and piezometric groundwater measurements (Liu and Wang, 2008). Surveys can be carried out by detecting surface movements of unstable areas through levels, theodolites, Electronic Distance Measurement, and total station GPS measurements (Liu Shao-tang, 2006). Remote control systems include aerial or terrestrial photogrammetry in the visible or radar ranges (Bitelli et al., 2004). Monitoring the distance between two points across the main landslide head scarp is the most effective way to describe the displacements within the landslide, at a site far away from its toe. This is particularly helpful in assessing the susceptibility of the whole landslide body to variations in toe conditions: in fact, a feedback at the head scarp helps to decipher the long range of these effects.

In November 2016, an international team of scientists, under the aegis of NATO, set about working in the area of the Enguri artificial water reservoir, on the southwestern foothills of the Greater Caucasus, Georgia (Fig. 1). During the first of several research missions, the team installed, for the first time in Georgia, two digital extensometers across the head scarp of the major, active Khoko landslide, located along the eastern mountain slope overlooking the reservoir. The associated hydroelectrical plant, built during the Soviet era (Fig. 1c), is responsible for about half of the energy supply to the country (Tibaldi et al. 2018). This monitoring activity is particularly relevant because the study area is located in a region affected by widespread seismicity (Fig. 1a), associated with still active mountain building processes, which have led to the formation of the Greater and Lesser Caucasus, resulting from the continent–continent collision between the African–Arabian and Eurasian plates (Reilinger 1997; 2006; Koçyigit et al. 2001; Pasquaré et al. 2011). Seismicity can produce earthquake with Ms of 6-7 (Tsereteli et al., 2016) and macroseismic intensities up to 10

(Varazanashvili et al., 2018), as a consequence of active compressional tectonics (Tsereteli et al., 2016; Tibaldi et al., 2017a, b, 2019). As broadly agreed upon in the scientific literature, there is a tight connection between active tectonic processes and the occurrence of landslides (e.g. Tibaldi et al. 2004, 2015; Tibaldi and Pasquaré, 2008; Pasquaré Mariotto and Tibaldi, 2016). As it is beyond doubt that, in the future, a seismic event will happen again in the area, the installed monitoring landslide system will be instrumental in quantitatively assessing the effects of ground shaking on slope deformation rate.

Last but not least, the Jvari-Khaishi-Mestia road cuts across the uppermost portion of the Khoko landslide, along a 2-km-long stretch, at an elevation of 700 m a.s.l. Several field surveys in the area enabled the team to assess the presence of developing cracks, shear planes, opening of holes, and an overall active deformation concentrated along 150-200-m-long road segments, which could pose serious threats to road traffic security. These fractured zones are being continuously repaired by way of asphalt refilling, with the purpose of preventing serious damage and road accidents.

We hereby provide and illustrate the database of measurements gathered by way of the integrated monitoring system installed at the Khoko landslide. The main goals of our research are to identify range and patterns of deformation, and assess possible relations between changes in water level at the artificial Enguri reservoir, meteorological factors (temperature and rain) and slope deformations. The analysis of these multi-temporal datasets is of broad interest, as it can provide a detailed framework for planning the most appropriate actions in the management of major water reservoirs aimed at energy production.

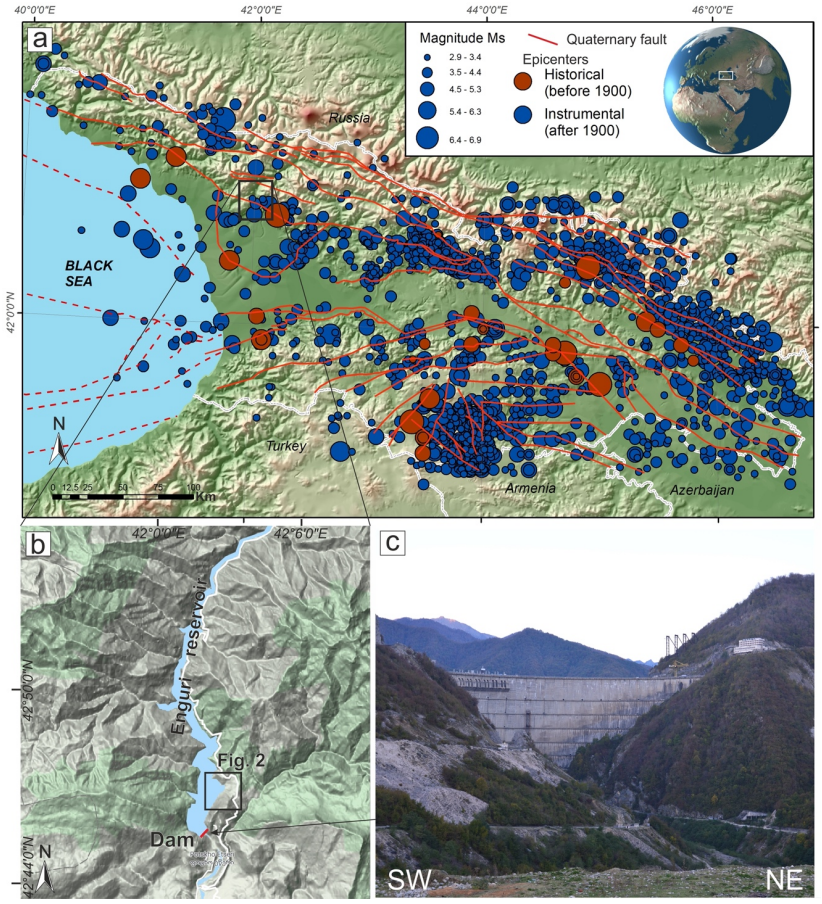

Figure 1. *(a) Main historic and instrumental earthquake epicenters in the western Greater Caucasus; the black rectangle shows the area of Figure (b). White lines are country borders; the main Quaternary faults (red lines) are from Gulen et al. (2011) and Tsereteli et al. (2016). Reference system: WGS84 / geographic coordinates. (b) DEM of the Enguri reservoir area, with dam location, © Google Maps. (c) Photo of the Enguri dam.*

2 Site description

2.1 Quaternary geology and geomorphology

The study area is characterized by substrate rocks and widespread Quaternary deposits, which have been mapped thanks to a new geological survey, integrated with geological maps compiled prior to the creation of the artificial lake (Fig. 2). The studied slope is marked by landforms that are typical of recent/active gravitational deformation; the total surface area affected by slope instability, which

is about 1.2 km^2, is characterized by debris, colluvium, alluvial, and ancient landslide deposits (Fig. 2) and fractured substrate rocks. Debris deposits are widespread in the lower parts of the mountain located in the southern sector of the study area, outside the landslide area. They can be observed also at the head scarp of the landslide. Colluvium deposits mantle the central part of the landslide body and the lowermost slope in the southwestern sector of the study area. Landslide deposits are widespread in the upper portion of the landslide body. Alluvial deposits are located along the trace of the old Enguri river, now below the artificial lake's level.

At an altitude of 720-740 m, a number of scarps can be noticed, facing westward and affecting the Jvari-Khaishi-Mestia road (Figs. 2 and 3). The height of such scarps ranges from 20 m to 70 m, representing the head scarps. These overall scarps cannot be the effect of roadcut during the road construction because these scarps are longer than the road, and thus the road only in part follows the scarp. In fact, the scarp prolongs outward from the road in the northern part. Moreover, the road cuts through the scarp in the southern part. Finally, the very large height of these scarps is poorly compatible with the supposed cut of a small road, especially considering that this scarp height is present also outside of the road. Anyway, some local modification of the lower part of the head scarp profile may have taken place during the road excavation. At the foot of the scarps, the topography is either horizontal or gently dipping westward, suggesting a possible uphill tilting of the slope (Fig. 3a). The asphalted surface of the road here is affected by fissures, as wide as a few centimeters, and by westward-facing, 20-cm-high (in 2016) scarps (Fig. 3d). These structures are parallel to sub-parallel to the morphological high head scarps. As documented by Tibaldi et al. (2019), in the forest across the southern segment of the head scarps, tens of meters long, and up to 3.8 m wide fissures were found. Some of the trees, with trunks of about 20 cm in diameter, grew inside the fissures, suggesting that the fissures have a long history, at least dating back to several tens of years (Tibaldi et al., 2019).

Downhill from the head scarp, several changes of inclination affect the slope, resulting in a series of downhill-facing scarps. Most are oriented perpendicularly to the local slope dip and can be observed in the upper part of the slope. This suggests the possible presence of secondary landslide slip planes (Tibaldi et al., 2019). Besides, most of the studied slope is characterized by the presence of several tilted trees; moreover, locally all of the trunks are tilted, and this is another indicator of active slope deformation (Fig. 3c).

The arrangement of river streams, as shown Figure 2, is based on the present-day river network and Soviet-era topographic maps compiled before the build-up of the water reservoir. In the slope section above the present-day lake, the rivers mostly follow the average slope dip, according to a dendritic pattern. Below the present-day lake level, one single stream was draining the landslide area. Here, at

Eliminato: deposits
Eliminato: deposits
Eliminato: deposits

the toe of the slope, this single stream was running parallel to the main Enguri river but with a northward, opposite flow (Tibaldi et al., 2019). This is an anomaly in the stream pattern that can be linked to a disturbance in the average slope topography, suggesting a possible early bulging of the landslide toe.

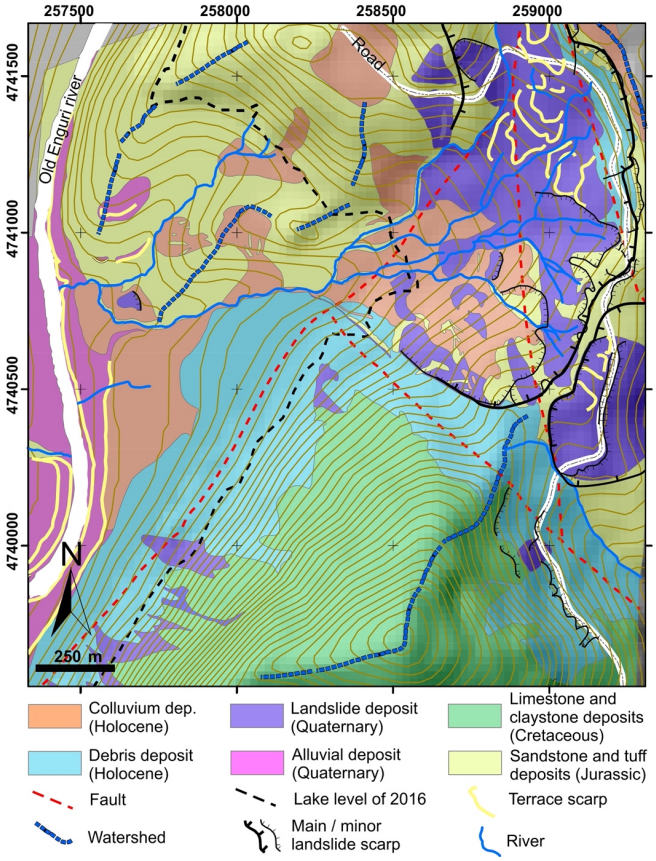

Figure 2. *Geological and geomorphological map of the study area, modified after Tibaldi et al. (2019). Location in Figure 1b.*

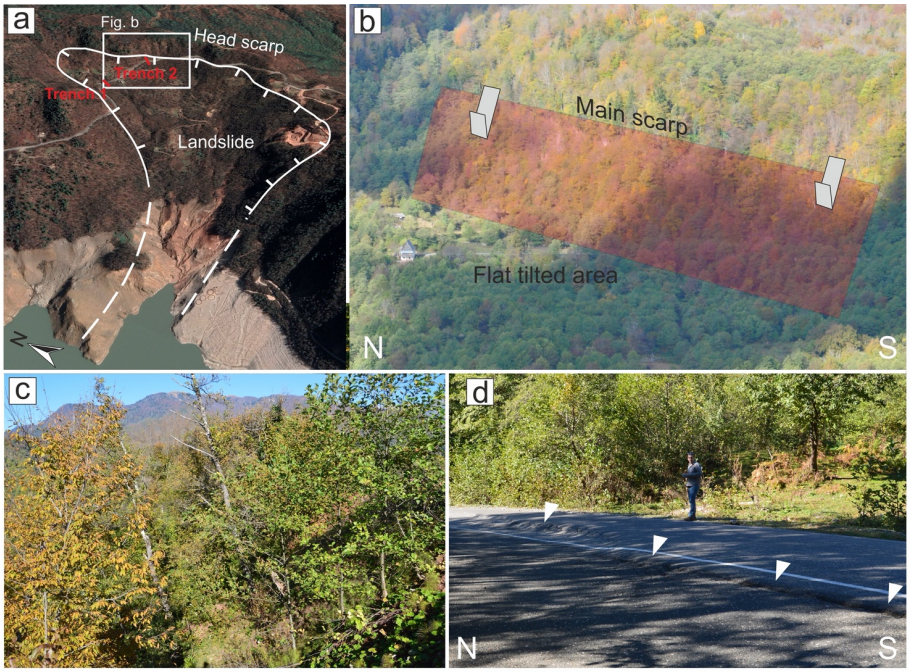

Figure 3. *(a) Oblique view of the studied landslide (© Google Earth); trench locations are shown. (b) Photo of a segment of the landslide head scarp; it is worth noticing the flat-lying area at the foot of the scarp, created by the uphill tilting of the slope during rotational movements of the landslide block. House for scale (left hand side of the flat area). (c) Example of tilted trees along the landslide slope. (d) Photo of the escarpments cutting the Jvari-Khaishi-Mestia road (white triangles), representing the surface expression of active landslide slip planes.*

2.2 Substrate description

Around the landslide area, Jurassic volcanic and terrigenous rocks and Cretaceous carbonate deposits crop out (Fig. 2), generally dipping to the south. The inclination of the Cretaceous strata cropping out around the Enguri dam is in the order of 60-70°, whereas the bedding attains a shallower dip northward, becoming sub-horizontal toward the northern part of the reservoir. Below the carbonate layers, Jurassic deposits can be observed, made of sandstones, tuffs, tuff-breccia and gypsum layers that crop out locally along the southeastern slopes of the reservoir. In the landslide area, essentially Jurassic and Quaternary deposits crop put. Here, most of the Jurassic rocks dip to the east, with slight variations (Fig. 4b). Presently, gypsum is excavated from a small mine, for economic purposes. Near

the coast of the artificial lake, at the foot of the onshore section of the landslide, there are intensely deformed gypsum rocks.

The complexity of the geometry of the head scarps as well as the morphology of the slope, and the size of the whole unstable slope, suggest that the landslide slip surface is not unique and probably there are different, partially superimposed slip planes. This interpretation is supported by the analysis of the state of preservation of piezometers originally installed in the landslide body. We checked the instruments and noticed that most of the piezometers installed during 2015 across the landslide, are interrupted at depths between 16 and 42 m (Table 1). Although the a priori hypothesis must be mentioned that these interruptions may have been produced by infiltration of fine material into the piezometers, we made the measurements in May 2017, only two years after their installation, thus the very recent age of the piezometers suggests that these may be the depths where the piezometric logs are intersected by the sliding surfaces of active landslides. This is supported by the observation that close piezometers, originally excavated down to different depths, are now interrupted at the same depth, such as BH3 and BH4 cut at -16 m, and BH1 and BH2 cut at -35-36 m. The fact that in general these ruptures are located at different depths indicates the presence of different slip planes.

Other logs were drilled during the Soviet era to reconstruct the rock distribution in the substrate. An analysis of the lithological characteristics of the logs shows that the intact substrate rock is located at deeper levels, in the order of several tens of meters. For example, logs 3261 and 3297 (drilled in 1966) (Fig. 4b) show the presence of clastic, unconsolidated deposits, rich in clay and locally gypsum fragments, down to a depth of 57.5 m (log 3297), and/or clastic deposits with a sill to clay matrix down to at least 61 m (log 3297) and at least 80 m (log 3261). Log 3291 (also drilled in 1966) shows the presence of clay and gypsum deposits down to a depth of 30 m, and of the substrate at greater depths. The geological survey integrated with the observations of the logs and piezometers enabled us to prepare the geological section of Figure 4b, which extends across the onshore landslide portion and below the lake (Fig. 4a). The section indicates that the intact substrate rock is always deeper than 30 m, down to 80 m. In this section, we added the head scarps of slip planes as observed in the field (red lines), and the main slip surfaces (dashed black lines) as obtained by a numerical slope analysis performed by Tibaldi et al. (2019). The analysis was carried out considering different levels of the lake reservoir; in the section are represented: i) the deepest slip surface (corresponding to FS < 1) among those obtained with a maximum of 510 m a.s.l. of the reservoir water level (this surface starts at log BH4), ii) the deepest slip surface (corresponding to FS < 1) among those calculated with a minimum of 430 m a.s.l. of the reservoir water level (this surface starts at log BH3), and iii) the shallowest slip surface that is present in both scenarios of lake level.

Eliminato: located

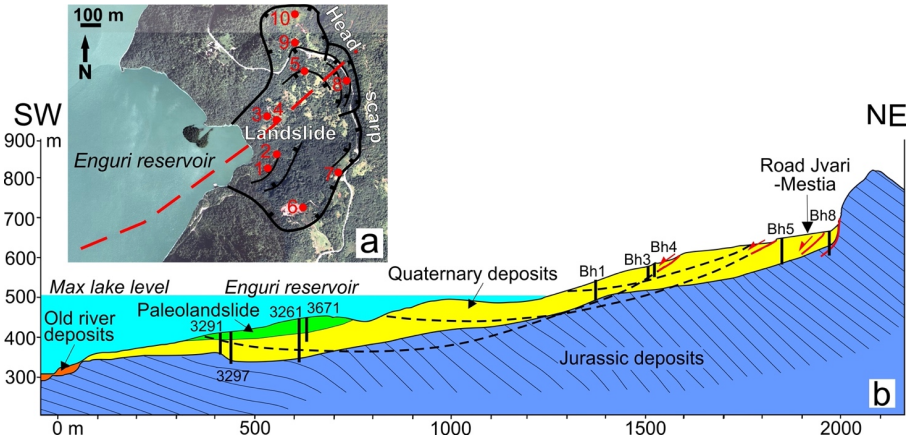

206
207

208 ***Figure 4.*** *(a) Trace (red dashed line) of the geological section and location (red dots) of the*
209 *piezometers described in Table 1. Black lines are major landslide scarps. (b) Geological section*
210 *across the slope facing the Enguri reservoir. Black columns represent locations and depth of logs*
211 *used to construct the cross section. Dashed black lines are the main potential slip surfaces calculated*
212 *through a static analysis by Tibaldi et al. (2019), red lines with arrows are landslide scarps surveyed*
213 *in the field. Data of the submerged part are derived from geological surveys made in the Soviet era,*
214 *before the construction of the dam.*

215

216 **Table 1.** Characteristics of measured piezometers and water table depth; b.g.s. refers to depths
217 below ground surface.

Site	Easting (dd.ddd)	Northing (dd.ddd)	Elevation (m)	Installed total depth (m b.g.s.)	Measured depth to water (m b.g.s.)	Measured depth to bottom (m b.g.s.)
BH1	42.049950	42.781550	566.6	45	7,4	35
BH2	42.050650	42.782500	568.2	50	1,5	36
BH3	42.049850	42.784583	587	32	1,3	16
BH4	42.050583	42.784417	652.8	65	1,3	16
BH5	42.052633	42.787150	679.7	50	0,5	42
BH6	42.053017	42.779717	725.9	50	12,0	18
BH7	42.055433	42.781700	721.3	50	5,8	49
BH8	42.055883	42.786517	704	55	4,8	23
BH9	42.051800	42.788767	702.6	51	0,2	37
BH10	42.051800	42.790167	727.9	50	Broken	Broken

3 Methodology and instrumentation

In 2016, two trenches were excavated across the main head scarps of the Khoko landslide, separated by about 240 m. The location of the sites selected for trenching is indicated in Figure 3a, and these locations were based upon the presence of clear indicators of active deformation on the road, at the foot of the main landslide scarps. Each of the two trenches was suitable for hosting a horizontal, digital extensometer (Wire Linear Potentiometric Transducer, SF500). The two trenches were opened perpendicularly to the scarp strike, crossing the road at a high angle (Fig. 5a). The instrumentation was placed within a protection system aimed at avoiding disturbance or damage from heavy load traffic (Figs. 5b-d). The opening of the trenches was performed in two stages, so as to enable vehicles to drive through the area along alternating lanes. The protection of the measurement stations consists of a channel in reinforced concrete, buried down to a depth of at least 50 cm.

The instrument is composed of a wire, a digital meter, and a recorder system. The stainless steel wire changes its length based on the relative movements of the piercing points to which it is connected. The wire was inserted into a pipe, laid down horizontally and protected with sand (Fig. 5c-d). At both ends, steel pipes were positioned, aimed at securing the measurement wire and the electronic instrumentation. Each vertical tube was equipped with a steel cover and gasket. The two covers were buried underneath a 15 cm-thick soil layer. These operations were made more difficult by the presence of a pavement in concrete beneath the present-day asphalt layer. The meter is a wire potentiometric position transducer that turns a linear motion into a resistance variation. It is made of a precision rotating potentiometer operated by the winding or unwinding stainless steel wire.

Due to the impossibility of transmitting the data directly to a computer at the Enguri dam premises or via internet (due to the remoteness of the site), the measurements have been stored in a digital recorder (data logger THEMIS-USB-GPRS) and downloaded on a 30-day basis. The system is connected to a set of insulated batteries with a life of 6 months.

Extensometer n. 1 was put in operation in November 2016, whereas the second extensometer began recording data in May 2017. The instruments include also an internal and external sensor of temperature - PT100.

The station for measuring the Enguri lake level is installed at an altitude of 360 m in the dam. It is made of a Multi-Channel Recorder RSG30 Ecograph T, by Endress+Hauser, using the Software ETU00xA, V2.02.xx. The data are transmitted in real-time to the dam administration and stored in local computers.

Rainfall amounts are recorded by a station, situated at an altitude of 540 m near the dam's administrative building. The station features the Davis Vantage Pro2 instrument, suitable for

measuring rainfall, wind speed, temperature and humidity, with data updated every 2.5 seconds. It comes with a self-emptying tipping spoon determining rainfall amounts in 0.2 mm increments, and is laser-calibrated for increasing accuracy. The data are transmitted in real-time to the dam administration and stored in local computers.

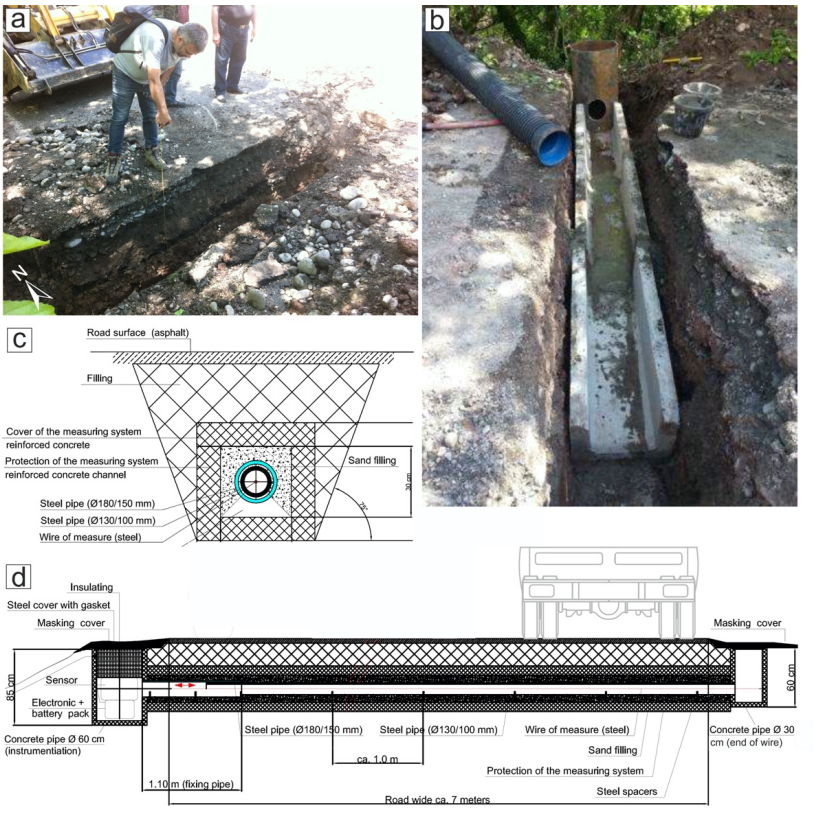

Figure 5*. (a) Opening of trench n. 1. (b) Installation of the concrete protection for the extensometer. (c) Section transversal to the extensometer system. (d) Longitudinal section of the extensometer system. Location of the two measurement stations provided in Figure 3a.*

4 Results

4.1 Extensometer data

The measurements here described reflect the real extension of this part of the slope, and cannot be related to the transit of heavy trucks along the road for the following reasons: the two instruments are

Eliminato: a

encapsulated in concrete boxes, and moreover between the instruments and the road asphalt there is a 50-cm-thick layer of reinforced concrete installed during the Soviet period. This clearly protects the extensometers from effects of trucks transit. Moreover, the extensometers recorded long periods of increase and decrease of extension movements, whereas trucks are always present.

Figure 6 shows the readings collected over a 35-month interval, between 4 November 2016 and 9 October 2019, by the extensometer at station n. 1. The overall extension recorded during the 35-month period is equal to 88.7 mm, corresponding to an average extension rate of 0.08 mm/day (that is 30.8 mm/y). Extension peaked from 16 May 2017 to 8 August 2017, with a total extension of 52 mm, corresponding to an average rate of 0.61 mm/day. This documented acceleration in the movement coincided with the opening of new fractures on the road surface at about 700 m of altitude, i.e. 230 m above the average lake level of 470 m a.s.l.

From 3 October 2017, extension ceased until 16 January 2018. This date marks the beginning of another period of slight extension, lasting until 6 March 2018. From this date on, another interval of extension rate increase was recorded, although much less pronounced than the previous one. This increase lasted until 22 May 2018, marked by a rate of 0.12 mm/day. From the end of May 2018 to October 2019, extension was linear with a rate of 0.04 mm/day, with a data gap between 30/12/2018 and 13/8/2019 due to a technical problem. This slower, creep-like movement was accompanied by the development of small sinkholes and fractures within the landslide body, which

occurred some tens of meters downslope of Trench 1.

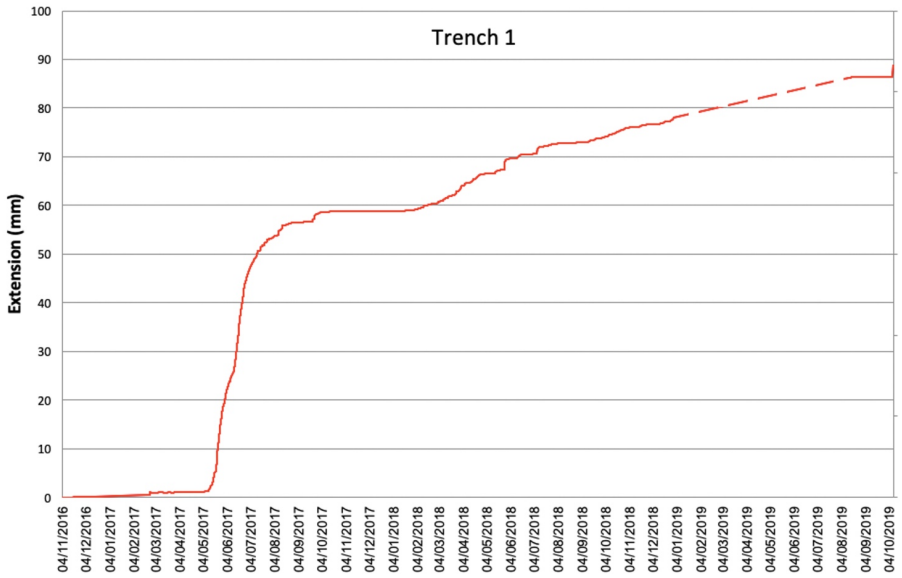

Figure 6. *Graph showing the readings of the incremental extension (in mm), associated with landslide surface displacement, recorded by station n.1 from November 2016 to October 2019.*

Regarding extensometer n. 2, data are shown over a 28.5-month interval (from 18 May 2017 to 30 September 2019) (Fig. 7). Here, the total amount of extension was 19.14 mm, with an average extension rate of 0.02 mm/day (that is 8.17 mm/y). From the beginning until 24 October 2017, there was a steady slight extension, followed by a period of high deformation expressed, in the graph, by a line with an upward convexity, indicating firstly a strong increase and later on a gradual decrease in the extension rate. This period lasted until 27 February 2018 and was characterized by an average rate of 0.16 mm/day, followed by another increase for one month, and then by a steady extension until 15 November 2018. Thereafter, until 29 January 2019, a new increase in the extension rate was observed, after which extension ceased.

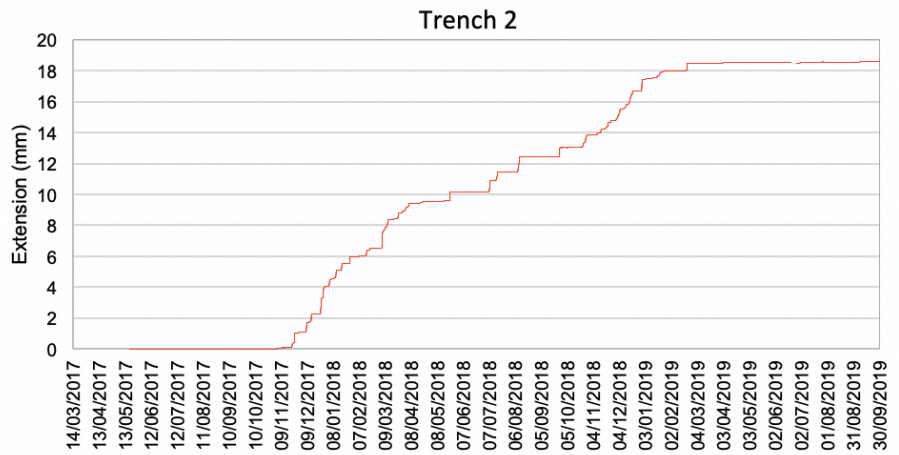

Figure 7. *Graph showing the readings of the incremental extension (in mm), associated with landslide surface displacement, and recorded from May 2017 to September 2019 by station n.2.*

4.2 Meteorological data

The amount of rainfall shows important variations (Fig. 8). Rainy days are mostly characterized by amounts within 10-20 mm/day. Peaks of 40-50 mm/day were recorded on 7/9/17, 5/2/18, 12/2/18, 26/9/18, 23/5/20 and 18/6/20. Peaks between 51-60 mm/day occurred on 6/12/17, 5/3/18 and 1/12/19. The highest peaks, above 70 mm/day, took place on 22/10/18 and 25/7/19. Periods of particularly heavy rains were recorded from 19/1/18 to 12/5/18 and from 22/9/18 to 16/1/19. From middle April 2018 to 25 September 2018, there was a gap in the data due to technical problems.

As regards temperatures (T), these show a double fluctuation (Fig. 9); the short-term fluctuation took place within a frequency of 5-20 days, whereas the long-term fluctuation developed each 12 months. At Trench 1, in the first period of observations, the T at the data logger, near the ground surface, gradually decreased to 3° on 22/2/17, though there was a gap in data, due to a technical problem, from mid- December 2017 to mid-February 2017. Then, T increased until it peaked to 22.9° on 15/8/17. From this date until 2/2/18, there was a gradual decrease, until a minimum of 5.5° was reached. Then T increased again and reached a maximum of 22.4° on 10/8/18. T then decreased down to 0.9° on 27/12/18. At Trench 2 the variations of T were similar to Trench 1, although the absolute values were sometimes higher, in the order of 1°-2°.

The T of the wire inside the instrument recorded the same pattern of variations, although smoothed, with T systematically higher, in the order of 3°-4° at Trench 1, and with a much smaller difference at Trench 2 (Fig. 9). This different pattern can be due to the fact that in Trench 2 there is a greater

circulation of water than in the other trench, and thus the temperature tends to be more balanced due to a better thermal conductivity of water than air.

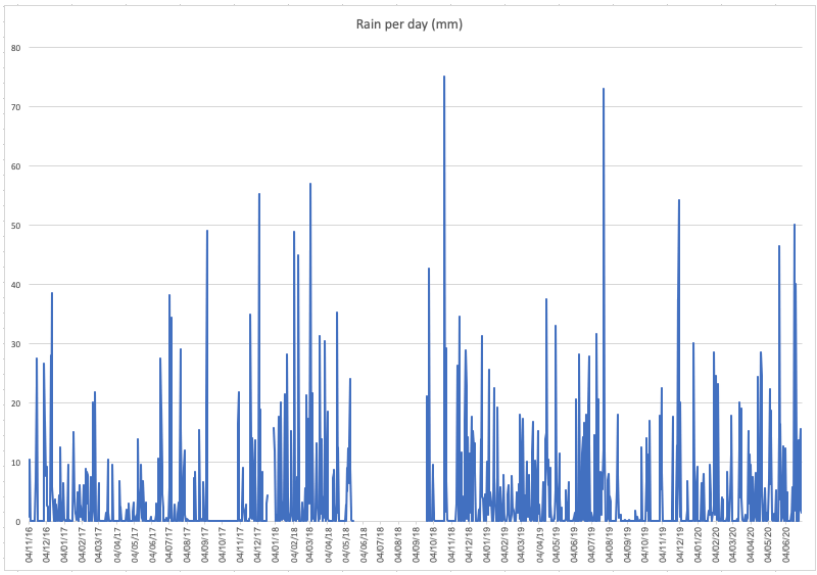

Figure 8. *Amount of rainfall recorded near the landslide, from 4 November 2016 to 30 June 2020.*

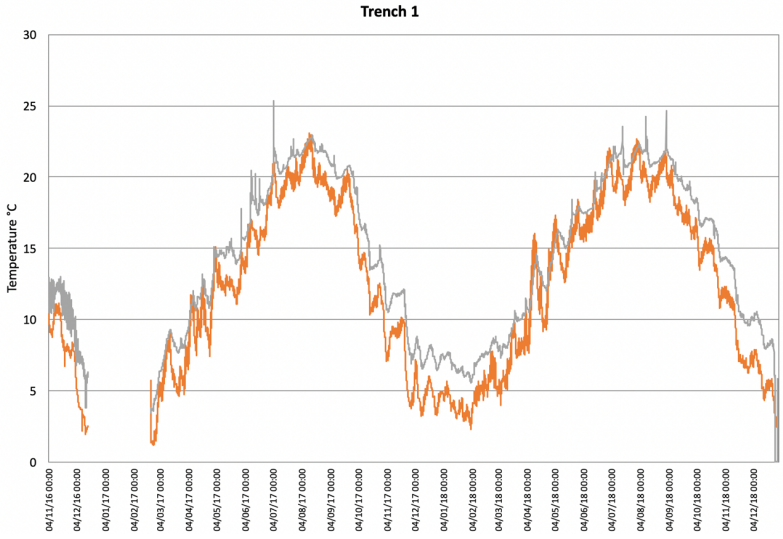

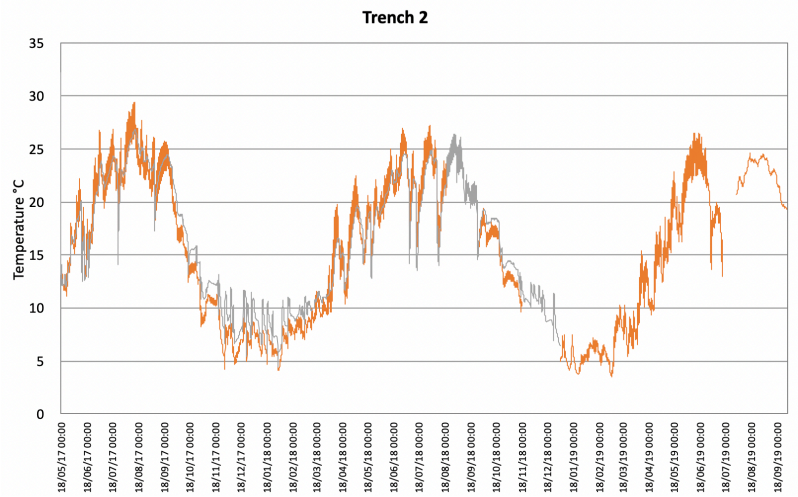

Figure 9. *Temperatures recorded at Trench 1 from November 2016 to December 2018, and at Trench 2 from May 2017 to September 2019. The grey line represents the variations in temperature of the extensometer wire, inside the instrument, whereas the orange line shows temperature variations at the data logger that is near the ground surface.*

4.3 Lake level data

Since the beginning of our measurements (1 January 2017) until 20 February 2017, there was a continuous emptying of the reservoir, the level of which dropped down to a minimum of 410 m a.s.l. (Fig. 10). Thereafter, the reservoir was filled again, to a maximum of 510 m on 5 August 2017, followed by a further increase on 12 September 2017, up to 511 m. From this date on, there was a decrease of the lake level until 29 February 2018, when it reached an altitude of 443 m. Then, it increased again reaching the altitude of 510 m on 30 June 2018. Later on, a new period of level decrease lasted until 31 March 2019, when lake level reached 414 m. Over the next month there was an oscillation with an increase of 35 m followed by a decrease. From 23 April 2019, a lake level increase was recorded, which ended on 26 July 2019, reaching an altitude of 507 m. Thereafter, a new period of lake level decrease took place, until 29 April 2020 when it reached 419 m.

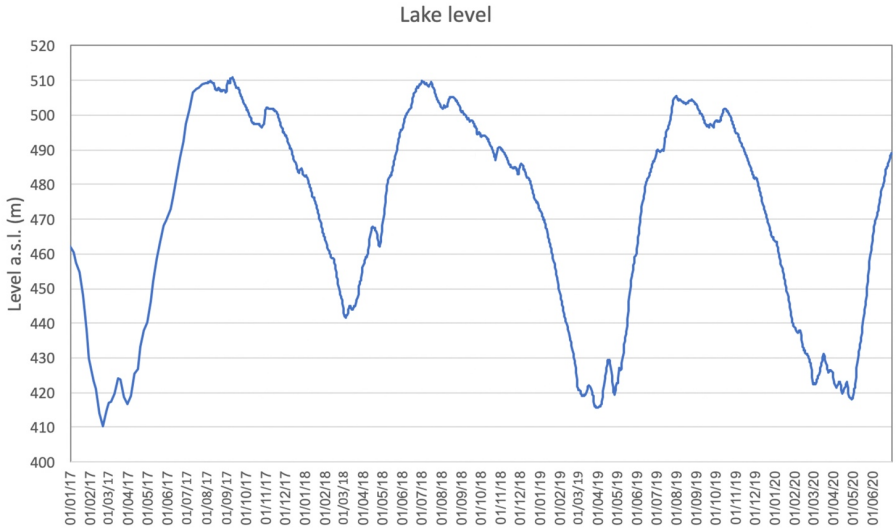

Figure 10. *Variations of the level of the Enguri artificial water reservoir from 1 January 2017 to 30 June 2020.*

5 Discussion

5.1 Correlation of slope deformation - lake level - rainfall

Here, we briefly discuss all the data, which we have combined in the graphs of Figure 11, so as to provide a more immediate interpretation. In this graph we also report the rainfall cumulated per month, in order to better quantify its possible influence. At extensometer n. 1, the total amount of extension has been 88.7 mm in 35 months, yielding an average extension rate of 0.08 mm/day. Extension peaked from 16 May 2017 to 8 August 2017, with a total extension of 52 mm that corresponds to a rate of 0.61 mm/day, about eight times the average extension rate during the whole measurement period. This extension rate increase follows the almost complete drawdown of the lake (which went down to the lowest level on 21 February 2017) and the ensuing period of lake level infilling, with a 100-m water level increase. A delay of about one month can be recognized between the lake level increase and the extension rate increase, but the shape and duration of the period of extension increase mimics exactly the shape and duration of the lake infilling (segments between arrows in Fig. 11), suggesting a strong correlation. Another interval of extensional rate increase, although much smoother than the previous one, is recognizable during a period after 6 March 2018, at the same time as a 67-m increase of the water level. During the third period of lake filling and refilling, due to technical problems at the extensometer, possible further rate variations were not

372 recorded. During periods of water level lowering, instead, the extension rate tends to decrease to the
373 lowest values.
374 At extensometer 1, there is no correlation between rainfall amounts and extension rate values in the
375 period 11/2016 – 4/2017, during which the extension curve is subhorizontal in spite of rainfall
376 variations. Similarly, there is no correlation between rain and extension when there is the strongest
377 extension increase of 5/2017 – 8/2017, because this follows a period of low rain precipitations. On
378 the contrary, this extension rate increase perfectly matches, after one month, the lake level increase.
379 The other period of extension increase from 2/2018 to 5/2018 coincides with the second lake level
380 increase, but it follows also a period of rainfall intensification (11/2017-2/2018). We suggest that, in
381 this case, cumulated rainfall might have contributed to increasing the extension rate owing to water
382 infiltration into the slope, though this is masked by lake level increase and we do not have data on the
383 variation of water saturation in the landslide slope.
384 At extensometer n. 2, the total amount of extension was 19.14 mm in 28.5 months, with an average
385 extension rate of 0.02 mm/day. There is no correlation between the amount of rainfall and extension
386 rate values in the period 5/2017 – 10/2017, during which the extension curve is subhorizontal in spite
387 of rainfall variations. Extension increased, from 31 October 2017 to 1 April 2018, to 0.13 mm/day,
388 corresponding to a 5-month interval of increased deformation, in a much similar way as at
389 extensometer n. 1, over a three-month period. It is worth noting that the extension curves derived
390 from the two extensometers have a similar shape, but at extensometer n. 2 the curve is shifted onward
391 by four to six months. This period of extension increase coincides with the lake level decrease, but it
392 also coincides with a period of rainfall increase. We suggest that these accelerated movements at
393 extensometer n. 2 may have been triggered by the previous movements within the landslide sector
394 where extensometer n. 1 is located, as it will be highlighted in the following chapter, in possible
395 combination with rain infiltration in the slope. At extensometer n. 2, the extension curve is still steep
396 in the following period until 7/2018, which is coincident with a lake level increase, followed by a
397 further extension rate increase until 1/2019, in correspondence of lake level decrease and strong
398 rainfall.
399 As documented by Tibaldi et al. (2019), based on the analysis of the Quaternary geological deposits
400 of the area, and by the presence of the high head scarp, the landslide area had already been subject to
401 slope failure events during prehistoric times. As a consequence of this, the processes that have taken
402 place along and across the slope during lake level variations, have been affecting an already
403 destabilized slope, which is expected to be more sensitive to variations of the conditions at its toe. In
404 general, the presence of artificial lakes can trigger possible seepage process accompanied by an
405 increase in pore water pressure in the slope deposits, with the effect of reducing their shear strength.

406 At the same time, the presence of a water basin may lead to a stabilization of the submerged part of
407 the slope (Paronuzzi et al., 2013). In transient conditions, lake filling or drawdown can trigger
408 landslides (Schuster, 1979; Kenney, 1992; Zhu et al., 2011). In a similar way to the Enguri case, pre-
409 existing, ancient landslides were reactivated during the filling of the water reservoir at the Włocławek
410 dam in Poland (Kaczmarek et al., 2015). This cause-effect relation is even more apparent, where
411 bank-forming materials have a high permeability, like in the study area, in which the slope is mostly
412 made of debris and highly fractured materials; within highly permeable deposits, a reservoir level
413 increase can trigger a rapid reservoir-induced water inflow that reduces both the strength and the
414 factor of safety. This occurred, for example, at the October 1963 Vajont landslide in NE Italy: as
415 documented by Paronuzzi et al. (2013), among the triggering factors for the disaster, a predominant
416 role was played by reservoir level increase, and by the presence of an already existing landslide.
417 Another example comes from the Byford Creek landslide, located above the Clyde artificial reservoir
418 in New Zealand, where lake filling produced a major increase in extension rate, followed by long-
419 term creep movements (Macfarlane, 2009).
420 To summarize the above, our data show that, at least during the first period of extension increase at
421 extensometer n. 1, the slope still has a high sensitivity to water infilling operations more than 40 years
422 after the construction of the Enguri reservoir. The presence of highly-permeable deposits in the lower
423 part of a slope, as is the case at the Khoko landslide, represents a key aspect to be considered for the
424 assessment of hydrogeological hazard. In such a case, during reservoir level increase, the water pore
425 pressure effects on shear strength prevail over the stabilizing and buttressing effects induced by the
426 water body, resulting in an acceleration in slope movements. For the other periods of extension
427 increase, an effect of rainfall intensification cannot be excluded, whereas extensometer n. 2 may also
428 have reacted to deformation of the slope part where the other extensometer n. 1 is located.
429

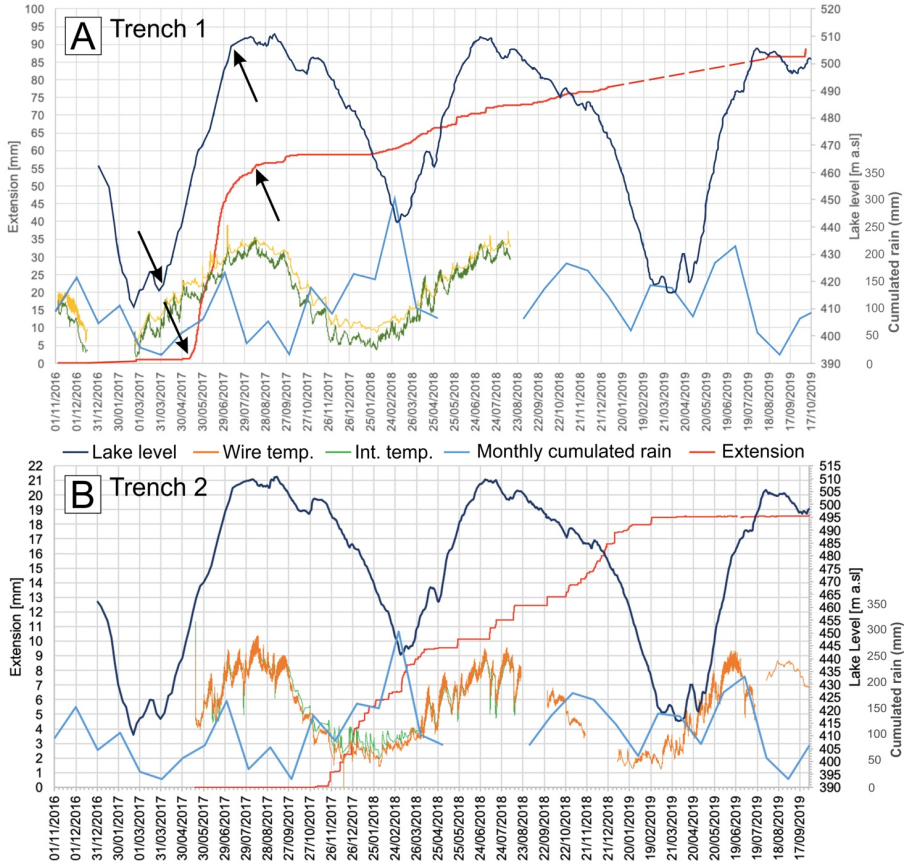

Figure 11. *Graphs showing the combination of all data collected at trench 1 (A) and trench 2 (B). Note that rainfall is expressed as cumulated month precipitation. The arrows point to the segments of the extension and lake level curves that show similar shape at short time distance.*

5.2 Behaviour of the landslide and slip planes

The hypothesis introduced in the previous chapter proposes that during the first and greatest lake level increase, there was an increment in water pore pressure within the slope with a consequent decrease of the shear strength. This seems to have produced an increase in extension at the two trenches with a time offset. Another possibility is that the lake level increase triggered slope deformation only at the landslide sector where extensometer n. 1 is located, whereas the other landslide portion, where extensometer n. 2 is located, initially remained stable but, later on, deformation was triggered also there. The different patterns observed at the two trenches may be explained in terms of the fact that

443 they are located in two different sectors of the general landslide, which can move separately. The
444 possible presence of different sectors within the general landslide body is suggested by underground
445 data and by GPS data. Based on the results summarized in Figure 4, a number of possible slip planes
446 affect the landslide, from shallow to deeper ones. Moreover, the slip planes modeled through our
447 static analysis are of two types: slip planes that initiate at the head scarp and prolong downward to
448 the valley bottom (now covered by the lake), and slip planes that run from the head scarp to half of
449 the slope, reaching the present lake's coastline. The presence of multiple slip planes at different depths
450 is supported also by the documented ruptures of piezometers at different depths. These slip planes
451 clearly correspond to different portions of the landslide that might move, at least in part,
452 autonomously from each other. GPS stations were installed in the upper part of the landslide and were
453 operational during most of the 2016-2019 observation period (Ospanov and Krivchenko, 2021). Four
454 GPS stations are characterized by motion vectors with the same cumulated magnitude of movement
455 (160-183 mm) and the same orientation (the central four arrows in Fig. 12), whereas the other two
456 GPS stations show different magnitude of movement (48 mm the GPS located west, and 80 mm the
457 GPS located east in Fig. 12) and different, opposite orientations. Based on these data and
458 geomorphological evidence, we suggest the possible presence of three main landslide sectors: two
459 corresponding to shallower landslides (A and B in Fig. 12) and one deeper (C in Fig. 12).
460 On the other hand, during the decrease of the lake level, extension increases at both trenches, as is
461 the case, for instance, at the very beginning of 2018. This increase in extension might be due to the
462 debuttressing of the slope toe associated with the emptying of the lake, resulting in a more widespread
463 mobilization of the landslide and probable inception of slip along the deeper planes. As already
464 suggested in the previous chapter, we cannot rule out the possibility that water infiltration due to
465 periods of increased rainfall might also have contributed to increasing the extension rate.
466

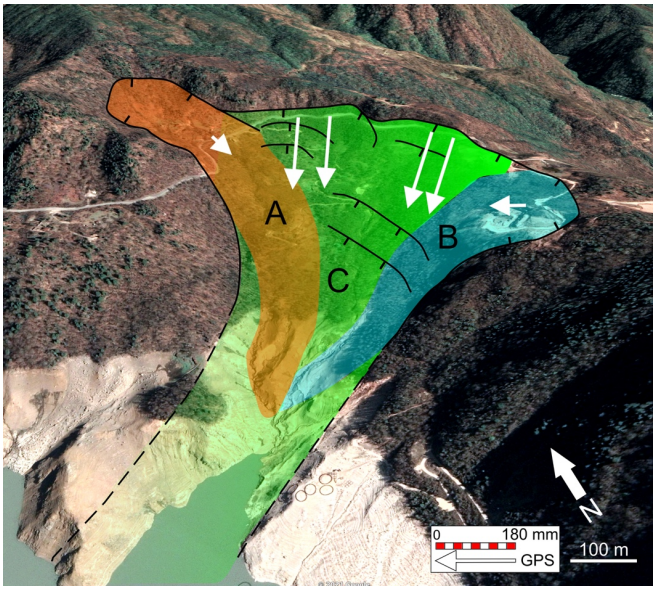

Figure 12. *Sketch of the possible different units that compose the general landslide onshore. The green unit C corresponds to a deeper-seated slope deformation, whereas the orange (A) and the blue (B) units are shallower bodies. White arrows represent GPS vectors collected by Ospanov and Krivchenko (2021). Black lines are the main scarps affecting the slope.*

6 Data availability

The databases showcased in this work are available for download from the UniData Repository (Milan, Italy) at https://www.unidata.unimib.it/?indagine=deformation-and-meteorological-data-of-the-khoko-landslide-enguri-republic-of-georgia-2016-2020, DOI: 10.20366/unimib/unidata/SI384-2.0 (Tibaldi et al., 2020). The extension dataset is provided in two separate files, for Trench 1 and for Trench 2, in tab format (extension data with frequency sampling of 60 min) together with air temperature near the ground surface (frequency sampling of 60 min), and temperature of the extensometer wire in the interior of the instrument (frequency sampling of 60 min). At the same web link is available the file of meteorological data (frequency sampling of 1 day) and lake level variations (frequency sampling each 5 days until 30/7/17 and then each one day).

7 Conclusions

At the major Khoko landslide, located on the eastern side of the Enguri artificial water reservoir, a 4-year-long campaign of measurement, by way of two digital extensometers, enables documenting the

Eliminato: DOI:

Eliminato: 10.20366/unimib/unidata/SI384-1.1

Formattato: SpazioDopo: 0 pt

activity of the mass movement, at a rate of 8.2 mm/yr to 30.8 mm/yr depending on the site of measurement. During this period, we observed a correlation between the greatest, rapid infilling of the lake and an increase in deformation rate of the slope. Deformation of the landslide at extensometer n. 1, thus, appears to have been controlled by variations in hydraulic load, induced mainly by lake oscillations. There is a systematic delay between man-induced lake oscillation and the response of the landslide mass, quantifiable in about one month at extensometer n. 1. Increase of extension at extensometer n. 2 may, in turn, have been triggered by the previous deformation that occurred in the landslide sector where the other extensometer is located. These results, together with the different slip rates at the two instruments, the presence of different slip planes at various depths, and the different orientations and amounts of movement measured at GPS stations located in the landslide, suggest that the Khoko landslide is composed of more than one unstable block, each of which can behave in a different way. Moreover, a possible correlation with heavier rainfall has been observed for some periods of increased extension, and thus we cannot rule out the possible contribution of water infiltration in the slope.

This overall monitoring effort will help individuate possible future accelerations of deformation at the unstable mass overlooking the Enguri artificial reservoir. Anyway, for a better comprehension of the instability of the whole slope, we recommend the installation of new inclinometers in the central and lower part of the slope.

Author contributions. AT coordinated the research and wrote most of the paper. PO designed and maintained the sensor network. FPM and FB contributed to the geological and geomorphological mapping of the landslide area. NT coordinated and contributed to collecting extension data at the extensometers. LM and JC provided meteorological and lake level data.

Competing interests. The authors declare they have no conflict of interest.

Acknowledgements. We are indebted to the Ministry of Infrastructure of Georgia that helped us to obtain the permission to work along the Jvari-Khaishi-Mestia road. We also wish to thank four anonymous reviewers for their precious and helpful comments and suggestions.

Financial support. This research was conducted with the financial help from NATO project SfP G4934 "Georgia Hydropower Security", the International Lithosphere Program - Task Force II, and project 216758 of the Shota Rustaveli National Science Foundation. Satellite images were provided in the framework of the European Space Agency project n. 32309 “Active tectonics and seismic hazard of southwest Caucasus by remotely-sensed and seismological data”.

References

Bertolini, G., Guida, M., & Pizziolo, M. (2005). Landslides in Emilia-Romagna region (Italy): strategies for hazard assessment and risk management. Landslides, 2(4), 302-312.

528 Bitelli, G., Dubbini, M., & Zanutta, A. (2004). Terrestrial laser scanning and digital photogrammetry
529 techniques to monitor landslide bodies. International Archives of Photogrammetry, Remote Sensing
530 and Spatial Information Sciences, 35(B5), 246-251.

531 Casagli, N., Tibaldi, A., Merri, A., Del Ventisette, C., Apuani, T., Guerri, L., Fortuny-Guasch J. &
532 Tarchi, D. (2009). Deformation of Stromboli Volcano (Italy) during the 2007 eruption revealed by
533 radar interferometry, numerical modelling and structural geological field data. Journal of
534 Volcanology and Geothermal Research, 182(3-4), 182-200.

535 Fell, R., Ho, K. K., Lacasse, S., & Leroi, E. (2005). A framework for landslide risk assessment and
536 management. Landslide risk management, 3-25.

537 Froude, M. J. and Petley, D. N., 2018. Global fatal landslide occurrence from 2004 to 2016, Nat.
538 Hazards Earth Syst. Sci., 18(8), 2161–2181, doi:10.5194/nhess-18-2161-2018.

539 Gulen L., and EMME WP2 Team (2011). Active faults and seismic sources of the Middle East region:
540 earthquake model of the Middle East (EMME) project. In: Abstracts of the AGU Fall Meeting, San
541 Francisco, California, 5-9 December 2011.

542 Kaczmarek, H., Tyszkowski, S., and Banach, M., 2015. Landslide development at the shores of a
543 dam reservoir (Włocławek, Poland), based on 40 years of research, Environmental Earth Sciences,
544 74(5), 4247-4259.

545 Kenney, T.C., 1992. Slope stability in artificial reservoirs: influence of reservoir level, selected cases,
546 and possible solutions, In: Semenza, E., Melidoro, G. (Eds.), Proceedings of the meeting on the 1963
547 Vajont landslide, 17-19 September 1986, Ferrara, Cansiglio and Vajont. Grafica Ferrarese, Ferrara,
548 Italy, 67-85.

549 Koçyigit, A., Yılmaz, A., Adamia, S., and Kuloshvili, S. (2001). Neotectonics of East Anatolia
550 Plateau (Turkey) and Lesser Caucasus: Implication for transition from thrusting to strike-slip faulting.
551 Geodin. Acta, 14, 177-195.

552 Liu Shao-tang 2006. Deformation measurements during the construction of large dam projects.
553 Chinese Journal of Underground Space and Engineering 06(Z2): 1346–1348.

554 Liu, S. T., and Wang, Z. W. (2008). Choice of surveying methods for landslides monitoring. In
555 Landslides and engineered slopes: from the past to the future. Proceedings of the tenth international
556 symposium on landslides and engineered slopes. Taylor & Francis, Xi'an.

557 Macfarlane, D.F., 2009. Observations and predictions of the behaviour of large, slow-moving
558 landslides in schist, Clyde Dam reservoir, New Zealand, Engineering Geology, 109(1-2), 5-15.

559 Ospanov N. S., and Krivchenko, A. A., 2021. Description of a 2-Year, High-Resolution Geodetic
560 Monitoring of the Khoko Landslide, Enguri Reservoir, Georgia. In. F. L. Bonali et al. (eds.), Building
561 Knowledge for Geohazard Assessment and Management in the Caucasus and other Orogenic
562 Regions, NATO Science for Peace and Security Series C: Environmental Security, Springer Nature,
563 301-316, doi.org/10.1007/978-94-024-2046-3_16.

564 Paronuzzi, P., Rigo, E., and Bolla, A., 2013. Influence of filling–drawdown cycles of the Vajont
565 reservoir on Mt. Toc slope stability, Geomorphology, 191, 75-93.

566 Pasquaré Mariotto F., Tibaldi A. (2016). nversion kinematics at deep-seated gravity slope
567 deformations revealed by trenching techniques. Nat. Hazards Earth Syst. Sci., 16, 663-674.

568 Pasquaré, F., Tormey, D., Vezzoli, L., Okrostsvaridze, A., Tutberidze, B. (2011). Mitigating the
569 consequences of extreme events on strategic facilities: Evaluation of volcanic and seismic risk
570 affecting the Caspian oil and gas pipelines in the Republic of Georgia. J. Environ. Man., 92, 1774–
571 1782.

572 Reilinger, R. E., McClusky, S. C., Oral, M. B., King, R. W., Toksoz, M. N., Barka, A. A., Kinik, I.,
573 Lenk, O., and Sanli, I. (1997). Global Positioning System measurements of present-day crustal
574 movements in the Arabia-Africa-Eurasia plate collision zone. J. Geophys. Res., 102, 9983–9999.

575 Reilinger, R. E., McClusky, S. C., Vernant, P., Lawrence, S., Ergintav, S., Cakmak, R., Ozener, H.,
576 Kadirov, F., Guliev, I., Stepanian, R., Nadariya, M., Hahubia, G., Mahmoud, S., Sakr, K., Arrajehi,
577 A., Paradissis, D., Al-Aydrus, A., Prilepin, M., Guseva, T., Evren, E., Dmirotsa, A., Filikov, S. V.,
578 Gomez, F., Al-Ghazzi, R., Karam, G. (2006). GPS constraints on continental deformation in the
579 Africa-Arabia-Eurasia continental collision zone and implications for the dynamics of plate
580 interactions. J. Geophys. Res., 111, B05411, https://doi.org/10.1029/2005JB004051.

581 Schuster, R.L., 1979. Reservoir-induced landslides, Bulletin of the International Association of
582 Engineering Geology, 20, 8-15.

583 Spiker, E. C., & Gori, P. (2003). National landslide hazards mitigation strategy, a framework for loss
584 reduction (No. 1244). US Geological Survey.

585 Tibaldi, A., Pasquaré F. (2008). Quaternary deformations along the "Engadine–Gruf tectonic
586 system", Swiss–Italian border. J. Quaternary Sci., 23 475–487.

587 Tibaldi, A., Rovida, A., Corazzato C. (2004). A giant deep-seated slope deformation in the Italian
588 Alps studied by paleoseismological and morphometric techniques. Geomorphology, 58, 27–47.

589 Tibaldi, A., Corazzato, C., Rust, D., Bonali, F. L., Pasquaré Mariotto, F., Korzhenkov, A. M., Oppizzi
590 P., and Bonzanigo, L. (2015). Tectonic and gravity-induced deformation along the active Talas–
591 Fergana Fault, Tien Shan, Kyrgyzstan. Tectonophysics, 657, 38–62.

592 Tibaldi, A., Alania, V., Bonali, F. L., Enukidze, O., Tsereteli, N., Kvavadze, N., Varazanashvili, O.
593 (2017a). Active inversion tectonics, simple shear folding and back-thrusting at Rioni Basin, Georgia.
594 J. Struct. Geol., 96, 35–53.

595 Tibaldi, A., Russo, E., Bonali, F.L., Alania, V., Chabukiani, A., Enukidze, O., Tsereteli, N. (2017b).
596 3-D anatomy of an active fault propagation fold: a multidisciplinary case study from Tsaishi
597 (Georgia), western Caucasus. Tectonophysics, 717, 253–269.

598 Tibaldi, A., Korzhenkov, A.M., Pasquaré Mariotto, F., Rust, D., Tsereteli, N. (2018). NATO and
599 earth scientists: An ongoing collaboration to assess geohazards and contribute to societal security in
600 Central Asia and the Caucasus. Episodes, 41, 193-205.

601 Tibaldi, A., Oppizzi, P., Gierke, J. S., Oommen, T., Tsereteli, N., Gogoladze, Z. (2019). Landslides
602 near Enguri dam (Caucasus, Georgia) and possible seismotectonic effects. Natural Hazards and Earth
603 System Sciences, 19, 71.

604 Tibaldi, A., Oppizzi, P., Bonali, F., Pasquarè Mariotto, F., Tsereteli, N., Mebonia, L., 2020.
605 Deformation and meteorological data of the Khoko landslide, Enguri, Republic of Georgia. UniData
606 - Bicocca Data Archive, Milan. Study Number SI384, Data file version 1.0 DOI:
607 10.20366/unimib/unidata/SI384-1.1

608 Tsereteli, N., Tibaldi, A., Alania, V., Gventsadse, A., Enukidze, O., Varazanashvili, O., Müller B. I.
609 R. (2016). Active tectonics of central-western Caucasus, Georgia. Tectonophysics, 691, 328-344.

610 Varazanashvili, O., Tsereteli, N., Bonali, F. L., Arabidze, V., Russo, E., Pasquaré Mariotto, F.,
611 Gogoladze, Z., Tibaldi, A., Kvavadze, N., Oppizzi, P. (2018). GeoInt: the first macroseismic intensity
612 database for the Republic of Georgia. J. Seismol., 1–43, https://doi.org/10.1007/s10950-017-9726-5.

613 Zhu, D., Yan, E., Hu, G., and Lin, Y. 2011. Revival deformation mechanism of Hefeng Landslide in
614 the Three Gorges Reservoir based on FLAC3D software, Procedia Engineering, 15, 2847-2851.